

## ACCEPTED VERSION

Chun-Chieh Chang, Daniel Headland, Derek Abbott, Withawat Withayachumnankul, and Hou-Tong Chen

### Demonstration of a highly efficient terahertz flat lens employing tri-layer metasurfaces

Optics Letters, 2017; 42(9):1867-1870

© 2017 Optical Society of America

Published version: <http://doi.org/10.1364/OL.42.001867>

#### PERMISSIONS

[https://www.osapublishing.org/submit/review/copyright\\_permissions.cfm#posting](https://www.osapublishing.org/submit/review/copyright_permissions.cfm#posting)

Reuse purpose	Article version that can be used under:		
	Copyright Transfer	Open Access Publishing Agreement	CC BY License
Reproduction by authors in a compilation or for teaching purposes short term	AM	VoR	VoR
Posting by authors on arXiv or other preprint servers after publication (posting of preprints before or during consideration is also allowed)	AM	VoR	VoR
Posting by authors on a non-commercial personal website or closed institutional repository (access to the repository is limited solely to the institutions' employees and direct affiliates (e.g., students, faculty), and the repository does not depend on payment for access, such as subscription or membership fees)	AM	VoR	VoR
Posting by authors on an open institutional repository or funder repository	AM after 12 month embargo	VoR	VoR
Reproduction by authors or third party users for non-commercial personal or academic purposes (includes the uses listed above and e.g. creation of derivative works, translation, text and data mining)	Authors as above, otherwise by permission only. Contact <a href="mailto:copyright@osa.org">copyright@osa.org</a> .	VoR	VoR
Any other purpose, including commercial reuse on such sites as ResearchGate, Academia.edu, etc. and/or for sales and marketing purposes	By permission only. Contact <a href="mailto:copyright@osa.org">copyright@osa.org</a> .	By permission only. Contact <a href="mailto:copyright@osa.org">copyright@osa.org</a>	VoR

10 December 2020

<http://hdl.handle.net/2440/105755>

# Demonstration of a highly efficient terahertz flat lens employing tri-layer metasurfaces

CHUN-CHIEH CHANG<sup>1,a)</sup>, DANIEL HEADLAND<sup>2,a)</sup>, DEREK ABBOTT<sup>2</sup>,  
WITHAWAT WITHAYACHUMNANKUL<sup>2</sup>, AND HOU-TONG CHEN<sup>1,\*</sup>

<sup>1</sup>Center for Integrated Nanotechnologies, Los Alamos National Laboratory, Los Alamos, NM 87545, USA

<sup>2</sup>School of Electrical and Electronic Engineering, The University of Adelaide, Adelaide, SA 5005, Australia

<sup>a)</sup>These authors contributed equally to this work

\* Electronic mail: chenht@lanl.gov

Compiled April 5, 2017

**We demonstrate a terahertz flat lens based on tri-layer metasurfaces allowing for broadband linear polarization conversion, where the phase can be tuned through a full  $2\pi$  range by tailoring the geometry of the sub-wavelength resonators. The lens functionality is realized by arranging these resonators to create a parabolic spatial phase profile. The fabricated 124  $\mu\text{m}$ -thick device is characterized by scanning the beam profile and cross section, showing diffraction-limited focusing and  $\sim 68\%$  overall efficiency at the operating frequency of 400 GHz. This device has potential for applications in terahertz imaging and communications, as well as beam control in general. © 2017 Optical Society of America**

*OCIS codes:* (230.0230) Optical devices; (230.4000) Optical devices, microstructure fabrication; (160.3918) Materials, metamaterials; (050.1965) Diffraction and gratings, Diffractive lenses; (110.6795) Imaging systems, terahertz imaging.

<https://doi.org/10.1364/OL.XX.XXXXXX>

Particular constraints in the terahertz range—namely historical difficulties in generating power [1], high atmospheric attenuation [2], and free-space path loss—result in a pronounced need for beam control devices in order to minimize power projected into unwanted directions [3]. Conventional geometric lenses and reflector devices are mature and readily available in the terahertz range, but their physical thickness and weight pose disadvantages. Compact, flat-profile beam control devices of subwavelength thickness are generally preferable for practical applications. A promising approach to realizing such devices is the use of metasurfaces [4–7] consisting of a planar array of heterogeneous elements that individually impart some particular phase shift to incident waves [8, 9]. The aggregation of these phases produces a wavefront that dictates the form of the ensuing propagating beam, and desirable behaviors have previously been demonstrated in transmission [10] or reflection [11–14] in the terahertz range. A full  $2\pi$  phase tunability range is required for optimal wave front engineering, and in transmission this typically necessitates the use of multiple layers of metallic

resonators [15–17], as a single layer is insufficient to support a magnetic resonance [18]. An alternative approach is to make use of the transmitted cross-polarization by employing anisotropic resonators [8], where the phase can be tuned by tailoring the resonator geometry, realizing functionality such as optical beam focusing [19, 20].

In the terahertz range, single-layer metasurface flat lenses have been demonstrated using C-shaped [21, 22] and complementary V-shaped resonators [23–26], which offer cross-polarized transmission efficiency below 25%, and in experiments the focusing efficiency was only a few percent. In previous work, the cross-polarization conversion efficiency was greatly enhanced by making use of additional non-resonant layers, and the tunable phase was exploited to enable a beam-steering device, with experimentally-demonstrated peak efficiency of 50–60% over a broad frequency range around  $\sim 1.2$  THz [27]. In the present work, we adapt this approach to create a highly efficient flat lens operating at around 400 GHz. The demonstrated flat lens is of practical value, as it can be employed to enhance antenna gain for high-volume communications [28], and focus radiation for imaging applications [29]. Additionally, the selection of an operating frequency toward the lower end of the terahertz range, as opposed to more terahertz-representative values such as 1 THz, is informed by lower absorption due to atmospheric gases [2], as well as a greater degree of compatibility with compact electronic terahertz sources and detectors [30, 31]. In principle, however, a metasurface of this sort can straightforwardly be scaled in size to serve higher frequencies, if desired.

Fig. 1(a) illustrates a unit cell of the metasurface, consisting of three layers of subwavelength metallic structures—two orthogonal wire grids and an array of anisotropic resonators in between. When the middle resonator is excited by the incident radiation polarized in the  $x$ -direction, the resultant electric dipole has a component that is orthogonal to the incident polarization, i.e., in the  $y$ -direction, and consequently, it radiates waves in the cross-polarization. Alternatively, we can understand that the anisotropic resonator is birefringent, converting the incident linear polarization to elliptical polarization and creating the cross-polarization component. The use of two non-resonant wire-grids forms a cavity to dramatically improve the efficiency

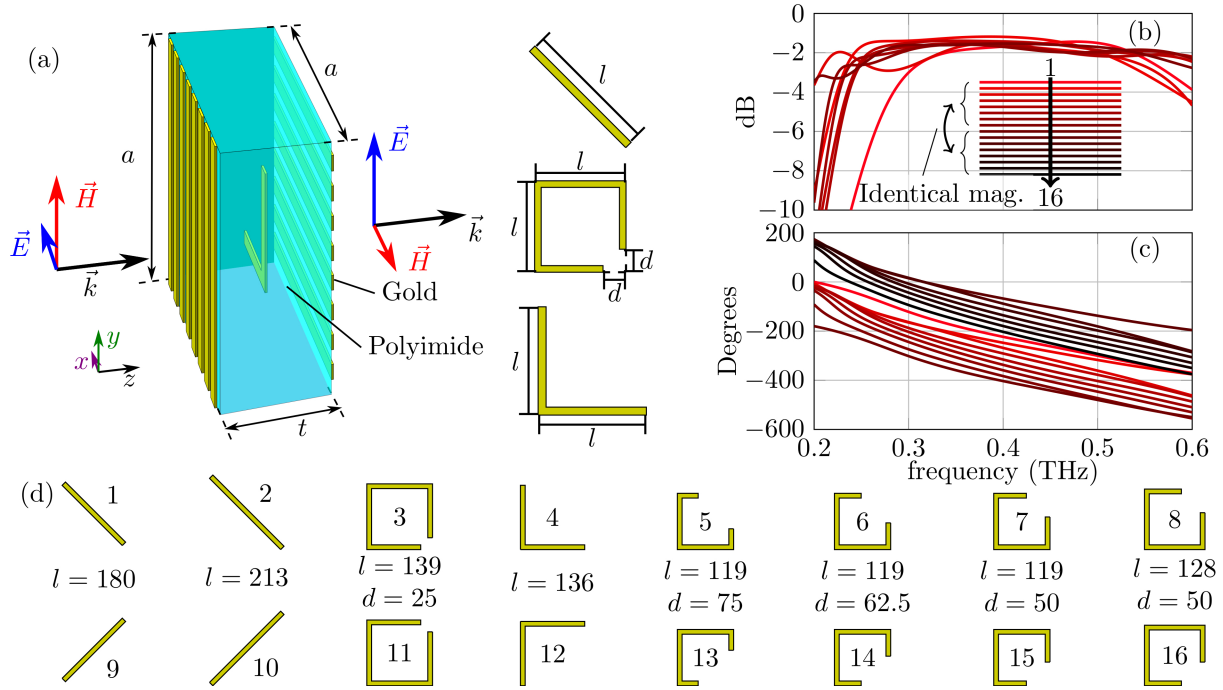


**Fig. 1.** (a) A unit cell structure of the tri-layer metasurface that allows for broadband linear polarization conversion, where  $a = 160 \mu\text{m}$  and  $t = 120 \mu\text{m}$ . The adjacent diagrams show three different classes of resonator shape used in this work. There are  $2\mu\text{m}$ -thick polyimide cap layers at the input and output surfaces, which are omitted for clarity. (b) Magnitude and (c) phase response of the cross-polarized transmission for the 16 resonator structures shown in (d). Note that resonators 9–16 formed by flipping resonators 1–8 in the  $x$ -axis. Consequently, their magnitude responses correspond identically, and are omitted from (b). Track width of all metal microstructures is  $10 \mu\text{m}$ , and the unit for the specified dimensions in (d) is  $\mu\text{m}$ .

of polarization conversion. Essentially, the front wire grid allows the incident waves to transmit through and interact with the resonator, and at the same time blocks the back-propagating waves with cross-polarization generated from the resonator. The back wire grid reflects the co-polarized waves back to the resonator for additional interactions, but allows the transmission of the cross-polarization. This enhances the conversion to cross-polarization in the forward direction, and ultimately there is only cross-polarized transmission (desirable) and co-polarized reflection (undesirable). The latter can be minimized by appropriately tuning the dielectric spacer thickness, which leads to destructive interference of multireflection from the metasurface cavity [32].

In principle, any anisotropic resonators can be applied in such tri-layer metasurfaces to achieve the linear polarization conversion. It has been shown that varying the resonator geometry can result in different transmission phases [27]. In this work we use three different basic resonator forms as shown in Fig. 1(a). The unit cell response is investigated with full-wave simulations using CST Microwave Studio, representing an infinite, uniform array of elements that is excited with normally-incident radiation. The obtained cross-polarized transmission magnitude and phase are plotted in Fig. 1(b) and (c), respectively, for a total of sixteen different resonators shown in Fig. 1(d). It can be seen from the results in Fig. 1(b) that the transmission efficiency at the nominal operating frequency of  $400 \text{ GHz}$  ranges from  $68\%$  to  $76\%$ , and it has at least  $50\%$  efficiency over a  $250 \text{ GHz}$  range that spans  $300 \text{ GHz}$  to  $550 \text{ GHz}$ , equivalent to  $62.5\%$  fractional bandwidth. More importantly, the phase response results in Fig. 1(c) show a smooth, near-linear phase gradient for all resonators, with an approximate phase step of  $\pi/8$  separating adjacent

phase responses across the entire usable frequency range. Note that resonators 9–16 are obtained by simply flipping resonators 1–8 in the  $x$ -axis, which alters their phase response by  $180^\circ$ , but with identical transmission magnitudes between corresponding resonators, as evidenced in Fig. 1(b,c).

In order to function as a lens, the metasurface must impart the following phase distribution onto the transmitted radiation [19],

$$\phi(r) = k_0(\sqrt{F^2 + r^2} - F), \quad (1)$$

where  $k_0$  is the free-space wavenumber,  $F$  is the desired focal length, and  $r$  is the distance from the center of the flat lens. It is noted that the engineering phase convention is made use of, in which a less-positive phase corresponds to a greater phase delay.

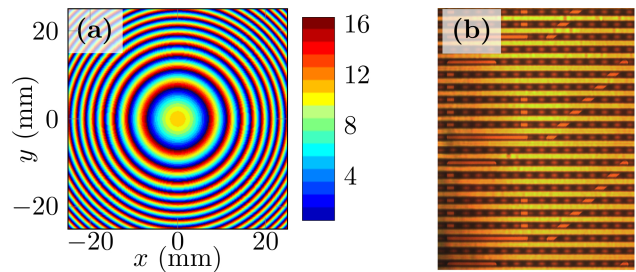


**Fig. 2.** (a) Spatial phase profile of the metasurface enabling lens function, where the color coding represents the use of different resonators listed in Fig. 1(d), spanning a full  $2\pi$  phase range. (b) A micrograph of a portion of the fabricated sample, showing two classes of resonators.

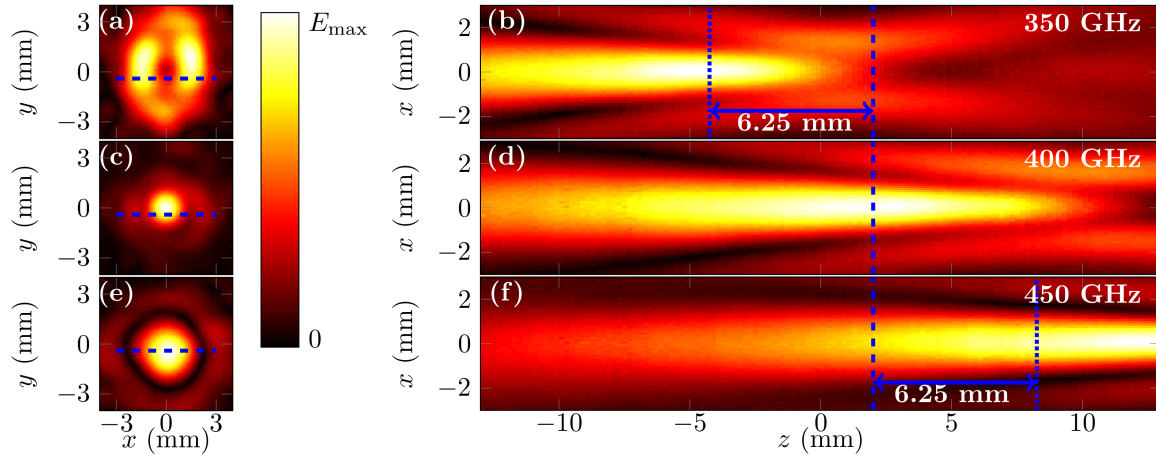


**Fig. 3.** Measured raster-scanned field distributions spanning a 100 GHz range around the nominal 400 GHz operating frequency. (a,c,e)  $xy$ -plane cross sections of the focused beam at 350, 400, and 450 GHz respectively, and (b,d,f)  $xz$ -plane beam profiles for corresponding frequencies. Blue dashed lines give the intersection between the  $xy$  and  $xz$  planes in each of the plots, and blue dotted lines give the expected location of the focal spots based on a simplified dispersion model. All field plots are normalized to their respective maxima, in linear scale.

This phase distribution can be mapped to the sixteen resonator designs via their discrete phase responses. For this design, a focal length of 50 mm at the nominal operating frequency of 400 GHz is selected, and the results of this procedure are given in Fig. 2(a).

The fabrication of the metasurface flat lens begins by spin-coating and thermal-curing a 2  $\mu\text{m}$ -thick polyimide layer (HD Microsystems PI-2525) onto a 4" Si substrate. A 200 nm-thick gold (Au) back grating (track width = 10  $\mu\text{m}$ ; duty cycle = 50%) is then fabricated using conventional contact lithography, electron-beam evaporation, and metal lift-off. A 60  $\mu\text{m}$ -thick polyimide layer is subsequently spin-coated and thermally cured on hotplates at 300°C for 150 minutes, with a temperature ramp of 2.5°C/min. The resonator array containing sixteen different classes of Au resonator is fabricated atop this polyimide layer, following the same steps used to realize the Au back grating. A second 60  $\mu\text{m}$ -thick polyimide layer is then spin-coated and thermally cured on top of the resonator layer, followed by the fabrication of the Au front grating, which is oriented orthogonally to the Au back grating. Another 2  $\mu\text{m}$ -thick polyimide cap layer is subsequently deposited and thermally cured in order to encapsulate the entire structure. Finally, the fabricated structure is mechanically peeled off from the Si substrate in order to establish a free-standing sample. A micrograph of a portion of the resulting sample is given in Fig 2(b), showing well-defined resonators and wire grids. The total area of the sample is  $\sim 50 \times 50 \text{ mm}^2$ , and hence there are a total of  $\sim 98,000$  individual resonator elements.

The sample is excited with a collimated beam of the appropriate polarization. The central portion of the incident beam is approximated by a Gaussian beam with a radius of 12 mm at the operating frequency, but it also exhibits some intrinsic, frequency-dependent irregularities. The cross-section ( $xy$ ) and profile ( $xz$ ) of the focused beam are raster-scanned, and results are presented in Fig. 3. Scans are presented at three frequencies of interest, namely 350 GHz, the designed operating frequency of 400 GHz, and 450 GHz. It is noted that the  $z$ -axis is defined relative to the focal plane at 400 GHz, rather than the flat lens device itself, as the realized focal distance is not explicitly known due to factors including divergence of the incident beam, as well

as the internal configuration of the detector PCA. It is apparent from the  $xy$ -scan that a focal spot is produced, shown in Fig. 3(c) at the operating frequency, and hence this validates the functionality of the nonuniform metasurface. The central portion of this focal spot is closely approximated by a narrow Gaussian beam, albeit with some un-desired fields surrounding the focus. These fields are associated with irregularities in the incident beam, which causes the output phase distribution to deviate from those specified by Equation (1). The beam diameter of the central portion is determined by curve fitting to be 2.3 mm, but it is worth noting that this is spread by the detector, which is approximated as a Gaussian aperture of diameter 1.32 mm. As such, the true beam diameter is determined to be  $\sim 1.88 \text{ mm}$ , which is close to the diffraction-limited value of  $\sim 1.98 \text{ mm}$  based on the input beam radius of 12 mm. From the  $xz$ -scan at the operating frequency presented in Fig. 3(d), the progression of the beam is revealed, and it can be seen that the beam passes through its focus, as expected. However, the aforementioned irregularities of the incident beam are also evident here, as the beam does not exhibit a strictly Gaussian intensity profile. For instance, there are sub-maxima at either side of the optical axis after it passes through its focus, which appear to correspond to the aforementioned un-desired fields surrounding the focus in the  $xy$ -scans in Fig. 3(c).

A flat lens of this sort is expected to be dispersive, given the approximately-proportional relationship between focal length and frequency for the frequency-invariant relative phase distribution. This is especially true given the near-constant difference in phase between resonator elements across the usable frequency range shown in Fig. 1(c). For this particular flat lens, this dispersion relation predicts a difference of  $\sim 6.25 \text{ mm}$  in focal length for a 50 GHz difference in frequency. As such, the  $xy$ -scans shown in Figures 3(a) and (e) are not at the device's focal plane, resulting in a broader spread in the electric field distribution. It is also worth noting that the scan in Fig. 3(a) shows an annular-like field distribution, which is ascribed to irregularities in the incident beam. The calculated focal plane positions for 350 and 400 GHz are consistent with the  $xz$ -scans given in Figures 3(b) and (d). However, the distance is greater for the scan shown in Fig. 3(f). We attribute this to frequency-dependent divergence of



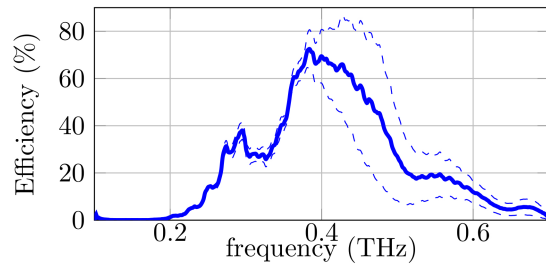


**Fig. 4.** Overall efficiency, investigated by single-pixel measurements, with error bars at one standard deviation given as dashed lines.

the incident beam, which exaggerates the spatial dispersion of the metasurface.

Of key interest to the performance of this device is the overall efficiency, and hence we evaluate this experimentally. The approach that we have employed is to compare the peak power delivered to the focal spot at 400 GHz with the power delivered by a standard polymethylpentene (TPX) lens of the same focal length serving as a reference. Discrepancies in output polarization and device aperture are compensated by setting the detector at a  $45^\circ$  angle, and passing the incident beam through an iris of  $\sim 25$  mm diameter, ensuring identical coverage of the incident terahertz beam. The dissipation and reflection losses of the reference lens are compensated analytically, based on material properties from the literature [33], and this measurement procedure is repeated five times in order to evaluate the associated degree of uncertainty. The results are presented in Fig. 4, revealing a mean peak efficiency of  $\sim 68\%$  at the nominal operating frequency of 400 GHz, which is consistent with the unit cell simulations. Additionally, we extract a  $-3$  dB spectral bandwidth of 150 GHz from these results, spanning from 340 to 490 GHz. It is also worth noting that the standard error increases markedly above the operating frequency, which is likely due to diminishing dynamic range with increase in frequency.

In summary, we have presented the design, fabrication, and characterization of a terahertz metasurface flat lens operating in the vicinity of 400 GHz. The demonstrated diffraction-limited focusing capability and operating frequency are amenable to practical applications including imaging and high-volume communications. The bandwidth of this device is mainly limited by spatial dispersion, and is found to be approximately 37%, which corresponds to 150 GHz of absolute spectral bandwidth. The transmission efficiency of the metasurface is experimentally evaluated to be  $\sim 68\%$  at the operating frequency.

**Acknowledgements** DA would like to thank the Australian Research Council (ARC) for providing funding via grants FT120100351 and DP140104651. We acknowledge support from the Los Alamos National Laboratory LDRD Program. The authors gratefully acknowledge John Nogan and Willard Ross for valuable discussion and assistance in device fabrication. This work was performed, in part, at the Center for Integrated Nanotechnologies, a U.S. Department of Energy, Office of Basic Energy Sciences Nanoscale Science Research Center operated jointly by Los Alamos and Sandia National Laboratories. Los Alamos National Laboratory, an affirmative action/equal opportunity employer, is operated by Los Alamos National Security, LLC, for the National Nuclear Security Administration of the U.S. Department of Energy under Contract No. DE-AC52-06NA25396.

## REFERENCES

- J. Chamberlain, *Philos. Trans. R. Soc., A* **362**, 199 (2004).
- ITU-R, "676-10 Attenuation by Atmospheric Gases," (2013).
- H.-J. Song and T. Nagatsuma, *IEEE Trans. THz Sci. Technol.* **1**, 256 (2011).
- H.-T. Chen, A. J. Taylor, and N. Yu, *Rep. Prog. Phys.* **79**, 076401 (2016).
- S. B. Glybovski, S. A. Tretyakov, P. A. Belov, Y. S. Kivshar, and C. R. Simovski, *Phys. Rep.* **634**, 1 (2016).
- N. Yu and F. Capasso, *Nat. Mater.* **13**, 139 (2014).
- A. V. Kildishev, A. Boltasseva, and V. M. Shalaev, *Science* **339**, 1232009 (2013).
- N. Yu, P. Genevet, M. A. Kats, F. Aieta, J.-P. Tetienne, F. Capasso, and Z. Gaburro, *Science* **334**, 333 (2011).
- S. Sun, Q. He, S. Xiao, Q. Xu, X. Li, and L. Zhou, *Nat. Mater.* **11**, 426 (2012).
- S.-G. Park, K. Lee, D. Han, J. Ahn, and K.-H. Jeong, *Appl. Phys. Lett.* **105**, 091101 (2014).
- T. Niu, W. Withayachumnankul, B. S.-Y. Ung, H. Menekse, M. Bhaskaran, S. Sriram, and C. Fumeaux, *Opt. Express* **21**, 2875 (2013).
- T. Niu, W. Withayachumnankul, A. Upadhyay, P. Gutruf, D. Abbott, M. Bhaskaran, S. Sriram, and C. Fumeaux, *Opt. Express* **22**, 16148 (2014).
- T. Niu, A. Upadhyay, W. Withayachumnankul, D. Headland, D. Abbott, M. Bhaskaran, S. Sriram, and C. Fumeaux, *Appl. Phys. Lett.* **107**, 031111 (2015).
- D. Headland, E. Carrasco, S. Nirantar, W. Withayachumnankul, P. Gutruf, J. Schwarz, D. Abbott, M. Bhaskaran, S. Sriram, J. Perruisseau-Carrier, and C. Fumeaux, *ACS Photonics* **3**, 1019 (2016).
- C. G. Ryan, M. R. Chaharmir, J. Shaker, J. R. Bray, Y. M. Antar, and A. Ittipiboon, *IEEE Trans. Antennas Propag.* **58**, 1486 (2010).
- C. Pfeiffer and A. Grbic, *IEEE Trans. Microw. Theory Techn.* **61**, 4407 (2013).
- L.-W. Chen, Y. Ge, and T. S. Bird, *Electron. Lett.* **52**, 1653 (2016).
- F. Monticone, N. M. Estakhri, and A. Alù, *Phys. Rev. Lett.* **110**, 203903 (2013).
- F. Aieta, P. Genevet, M. A. Kats, N. Yu, R. Blanchard, Z. Gaburro, and F. Capasso, *Nano Lett.* **12**, 4932 (2012).
- X. Ni, S. Ishii, A. V. Kildishev, and V. M. Shalaev, *Light: Sci. Appl.* **2**, e72 (2013).
- X. Zhang, Z. Tian, W. Yue, J. Gu, S. Zhang, J. Han, and W. Zhang, *Adv. Mater.* **25**, 4567 (2013).
- Q. Wang, X. Zhang, Y. Xu, Z. Tian, J. Gu, W. Yue, S. Zhang, J. Han, and W. Zhang, *Adv. Opt. Mater.* **3**, 779 (2015).
- D. Hu, X. Wang, S. Feng, J. Ye, W. Sun, Q. Kan, P. J. Klar, and Y. Zhang, *Adv. Opt. Mater.* **1**, 186 (2013).
- X.-Y. Jiang, J.-S. Ye, J.-W. He, X.-K. Wang, D. Hu, S.-F. Feng, Q. Kan, and Y. Zhang, *Opt. Express* **21**, 30030 (2013).
- J. He, X. Wang, D. Hu, J. Ye, S. Feng, Q. Kan, and Y. Zhang, *Opt. Express* **21**, 20230 (2013).
- D. Hu, G. Moreno, X. Wang, J. He, A. Chahadih, Z. Xie, B. Wang, T. Akalin, and Y. Zhang, *Opt. Commun.* **322**, 164 (2014).
- N. K. Grady, J. E. Heyes, D. R. Chowdhury, Y. Zeng, M. T. Reiten, A. K. Azad, A. J. Taylor, D. A. Dalvit, and H.-T. Chen, *Science* **340**, 1304 (2013).
- X. Yu, R. Asif, M. Piels, D. Zibar, M. Galili, T. Morioka, P. U. Jepsen, and L. K. Oxenløwe, *IEEE Trans. THz Sci. Technol.* **6**, 765 (2016).
- E. Ojefors, U. R. Pfeiffer, A. Lisauskas, and H. G. Roskos, *IEEE J. Solid-State Circuits* **44**, 1968 (2009).
- U. R. Pfeiffer, Y. Zhao, J. Grzyb, R. Al Hadi, N. Sarmah, W. Förster, H. Rucker, and B. Heinemann, *IEEE J. Solid-State Circuits* **49**, 2938 (2014).
- J. Grzyb, B. Heinemann, and U. R. Pfeiffer, *IEEE J. Solid-State Circuits* **51**, 3063 (2016).
- H.-T. Chen, *Opt. Express* **20**, 7165 (2012).
- A. Podzorov and G. Gallot, *Appl. Opt.* **47**, 3254 (2008).

## REFERENCES

1. J. Chamberlain, "Where optics meets electronics: Recent progress in decreasing the terahertz gap," *Philos. Trans. R. Soc., A* **362**, 199–213 (2004).
2. ITU-R, "676-10 Attenuation by Atmospheric Gases," (2013).
3. H.-J. Song and T. Nagatsuma, "Present and future of terahertz communications," *IEEE Trans. THz Sci. Technol.* **1**, 256–263 (2011).
4. H.-T. Chen, A. J. Taylor, and N. Yu, "A review of metasurfaces: Physics and applications," *Rep. Prog. Phys.* **79**, 076401 (2016).
5. S. B. Glybovski, S. A. Tretyakov, P. A. Belov, Y. S. Kivshar, and C. R. Simovski, "Metasurfaces: From microwaves to visible," *Phys. Rep.* **634**, 1–72 (2016).
6. N. Yu and F. Capasso, "Flat optics with designer metasurfaces," *Nat. Mater.* **13**, 139–150 (2014).
7. A. V. Kildishev, A. Boltasseva, and V. M. Shalaev, "Planar photonics with metasurfaces," *Science* **339**, 1232009 (2013).
8. N. Yu, P. Genevet, M. A. Kats, F. Aieta, J.-P. Tetienne, F. Capasso, and Z. Gaburro, "Light propagation with phase discontinuities: Generalized laws of reflection and refraction," *Science* **334**, 333–337 (2011).
9. S. Sun, Q. He, S. Xiao, Q. Xu, X. Li, and L. Zhou, "Gradient-index metasurfaces as a bridge linking propagating waves and surface waves," *Nat. Mater.* **11**, 426–431 (2012).
10. S.-G. Park, K. Lee, D. Han, J. Ahn, and K.-H. Jeong, "Subwavelength silicon through-hole arrays as an all-dielectric broadband terahertz gradient index metamaterial," *Appl. Phys. Lett.* **105**, 091101 (2014).
11. T. Niu, W. Withayachumnankul, B. S.-Y. Ung, H. Menekse, M. Bhaskaran, S. Sriram, and C. Fumeaux, "Experimental demonstration of reflectarray antennas at terahertz frequencies," *Opt. Express* **21**, 2875–2889 (2013).
12. T. Niu, W. Withayachumnankul, A. Upadhyay, P. Gutruf, D. Abbott, M. Bhaskaran, S. Sriram, and C. Fumeaux, "Terahertz reflectarray as a polarizing beam splitter," *Opt. Express* **22**, 16148–16160 (2014).
13. T. Niu, A. Upadhyay, W. Withayachumnankul, D. Headland, D. Abbott, M. Bhaskaran, S. Sriram, and C. Fumeaux, "Polarization-dependent thin-film wire-grid reflectarray for terahertz waves," *Appl. Phys. Lett.* **107**, 031111 (2015).
14. D. Headland, E. Carrasco, S. Nirantar, W. Withayachumnankul, P. Gutruf, J. Schwarz, D. Abbott, M. Bhaskaran, S. Sriram, J. Perruisseau-Carrier, and C. Fumeaux, "Dielectric resonator reflectarray as high-efficiency nonuniform terahertz metasurface," *ACS Photonics* **3**, 1019–1026 (2016).
15. C. G. Ryan, M. R. Chaharmir, J. Shaker, J. R. Bray, Y. M. Antar, and A. Ittipiboon, "A wideband transmitarray using dual-resonant double square rings," *IEEE Trans. Antennas Propag.* **58**, 1486–1493 (2010).
16. C. Pfeiffer and A. Grbic, "Millimeter-wave transmitarrays for wavefront and polarization control," *IEEE Trans. Microw. Theory Techn.* **61**, 4407–4417 (2013).
17. L.-W. Chen, Y. Ge, and T. S. Bird, "Ultrathin flat microwave transmitarray antenna for dual-polarised operations," *Electron. Lett.* **52**, 1653–1654 (2016).
18. F. Monticone, N. M. Estakhri, and A. Alù, "Full control of nanoscale optical transmission with a composite metascreen," *Phys. Rev. Lett.* **110**, 203903 (2013).
19. F. Aieta, P. Genevet, M. A. Kats, N. Yu, R. Blanchard, Z. Gaburro, and F. Capasso, "Aberration-free ultrathin flat lenses and axicons at telecom wavelengths based on plasmonic metasurfaces," *Nano Lett.* **12**, 4932–4936 (2012).
20. X. Ni, S. Ishii, A. V. Kildishev, and V. M. Shalaev, "Ultra-thin, planar, babinet-inverted plasmonic metalenses," *Light: Sci. Appl.* **2**, e72 (2013).
21. X. Zhang, Z. Tian, W. Yue, J. Gu, S. Zhang, J. Han, and W. Zhang, "Broadband terahertz wave deflection based on C-shape complex metamaterials with phase discontinuities," *Adv. Mater.* **25**, 4567–4572 (2013).
22. Q. Wang, X. Zhang, Y. Xu, Z. Tian, J. Gu, W. Yue, S. Zhang, J. Han, and W. Zhang, "A broadband metasurface-based terahertz flat-lens array," *Adv. Opt. Mater.* **3**, 779–785 (2015).
23. D. Hu, X. Wang, S. Feng, J. Ye, W. Sun, Q. Kan, P. J. Klar, and Y. Zhang, "Ultrathin terahertz planar elements," *Adv. Opt. Mater.* **1**, 186–191 (2013).
24. X.-Y. Jiang, J.-S. Ye, J.-W. He, X.-K. Wang, D. Hu, S.-F. Feng, Q. Kan, and Y. Zhang, "An ultrathin terahertz lens with axial long focal depth based on metasurfaces," *Opt. Express* **21**, 30030–30038 (2013).
25. J. He, X. Wang, D. Hu, J. Ye, S. Feng, Q. Kan, and Y. Zhang, "Generation and evolution of the terahertz vortex beam," *Opt. Express* **21**, 20230–20239 (2013).
26. D. Hu, G. Moreno, X. Wang, J. He, A. Chahadih, Z. Xie, B. Wang, T. Akalin, and Y. Zhang, "Dispersion characteristic of ultrathin terahertz planar lenses based on metasurface," *Opt. Commun.* **322**, 164–168 (2014).
27. N. K. Grady, J. E. Heyes, D. R. Chowdhury, Y. Zeng, M. T. Reiten, A. K. Azad, A. J. Taylor, D. A. Dalvit, and H.-T. Chen, "Terahertz metamaterials for linear polarization conversion and anomalous refraction," *Science* **340**, 1304–1307 (2013).
28. X. Yu, R. Asif, M. Piels, D. Zibar, M. Gallii, T. Morioka, P. U. Jepsen, and L. K. Oxenlöwe, "400-GHz wireless transmission of 60-Gb/s Nyquist-QPSK signals using UTC-PD and heterodyne mixer," *IEEE Trans. THz Sci. Technol.* **6**, 765–770 (2016).
29. E. Ojefors, U. R. Pfeiffer, A. Lisauskas, and H. G. Roskos, "A 0.65 THz focal-plane array in a quarter-micron CMOS process technology," *IEEE J. Solid-State Circuits* **44**, 1968–1976 (2009).
30. U. R. Pfeiffer, Y. Zhao, J. Grzyb, R. Al Hadi, N. Sarmah, W. Förster, H. Rucker, and B. Heinemann, "A 0.53 THz reconfigurable source module with up to 1 mW radiated power for diffuse illumination in terahertz imaging applications," *IEEE J. Solid-State Circuits* **49**, 2938–2950 (2014).
31. J. Grzyb, B. Heinemann, and U. R. Pfeiffer, "A 0.55 THz near-field sensor with a  $\mu\text{m}$ -range lateral resolution fully integrated in 130 nm sige BiCMOS," *IEEE J. Solid-State Circuits* **51**, 3063–3077 (2016).
32. H.-T. Chen, "Interference theory of metamaterial perfect absorbers," *Opt. Express* **20**, 7165–7172 (2012).
33. A. Podzorov and G. Gallot, "Low-loss polymers for terahertz applications," *Appl. Opt.* **47**, 3254–3257 (2008).